

Article

Evolution of Microstructure and Mechanical Properties of Novel Al-Mg-Mn-Ag-Cr-Zr Alloy

Huan Wang ¹, Tao Liu ², Yanli Wu ² and Cheng Guo ^{1,*}¹ School of Mechanical Engineering, Yanshan University, Qinhuangdao 066004, China² MCC Heavy Industry (Tangshan) Co., Ltd., Tangshan 063000, China

* Correspondence: chengguo@ysu.edu.cn; Tel.: +86-132-3404-0860

Abstract: In order to reinforce the mechanism of Ag in 5xxx aluminum alloys with low magnesium, research on the microstructure and mechanical properties of an Al-Mg-Mn-Ag-Cr-Zr alloy was conducted using optical microscopy (OM), scanning electron microscopy (SEM), transmission electron microscopy (TEM), hardness measurement, and tensile testing. The as-cast microscopic structure of the alloy comprises the Al₆(Mn, Fe) phase and the T-Mg₃₂(Al, Ag)₄₉ phase. Changes in the characteristics of the investigated alloy were clear during the aging process. Based on the findings obtained from TEM and SAED analysis, it was evident that the predominant strengthening phase during the peak-aged stage is the β'' phase, observed when the alloy is aged for 24 h at 160 °C. The β'' phase had a L1₂-type crystal lattice architecture and presented a completely coherent relevance with the Al-matrix. The lattice parameter, *a*, of the β'' phase was 0.408 nm. The mechanical properties of the peak-aged alloy increased greatly as compared to the as-quenched alloy. The tensile strength exhibited a rise from 410 MPa to 449 MPa, representing a 9.5% increase, while the yield strength demonstrated an increase from 185 MPa to 273 MPa, indicating a significant enhancement of 47.5%. The method used in the present study has solved the problem of 5xxx aluminum alloys not being heat treatable for strengthening to a significant degree, considerably improving the alloy strength. In addition, new methods and foundations for exploiting new-type Al-Mg based alloys and developing high-strength aluminum alloys are provided in this study.

Keywords: peak-aged stage; β'' phase; L1₂ structure; mechanical properties



Citation: Wang, H.; Liu, T.; Wu, Y.; Guo, C. Evolution of Microstructure and Mechanical Properties of Novel Al-Mg-Mn-Ag-Cr-Zr Alloy. *Coatings* **2024**, *14*, 134. <https://doi.org/10.3390/coatings14010134>

Received: 20 December 2023

Revised: 16 January 2024

Accepted: 17 January 2024

Published: 19 January 2024



Copyright: © 2024 by the authors. Licensee MDPI, Basel, Switzerland. This article is an open access article distributed under the terms and conditions of the Creative Commons Attribution (CC BY) license (<https://creativecommons.org/licenses/by/4.0/>).

1. Introduction

In order to address escalating carbon dioxide emissions within the transportation sector, there is an urgent need for the development of quality low-density materials in the field of transportation, such as in high-speed railways, ships, and automobiles. Hence, it is imperative to focus on research and development endeavors dedicated to high-performance lightweight materials. At present, aluminum alloys, as low-density metal materials with high specific strength, have a strong application market. Recent research and development challenges faced in the arena of low-density high-performance materials have been related to the tradeoff among strength, ductility, and corrosion resistance.

5xxx series aluminum alloys (Al-Mg based alloys) have high specific strength, low density, and great corrosion resistance. They have a wide range of applications in the marine field and in automotive structural components [1]. However, as the 5xxx series aluminum alloys are classified as non-heat treatable aluminum alloys, their mechanical properties are notably inferior compared to heat treatable aluminum alloys. Methods used to enhance the strength of the 5xxx series aluminum alloys include work hardening and solid solution strengthening. Cold deformation can improve the work hardening effect by increasing the number and density of dislocations. Expanding the Mg content in 5xxx series aluminum alloys can also improve solid solution strengthening. However, cold deformation and raising the proportion of Mg element in these alloys promotes the precipitation of the β phase (Al₃Mg₂) alongside

crystal boundaries. As a result, the ductility and the corrosion performance of the alloys deteriorate. Therefore, developing a new 5xxx series aluminum alloy which is heat treatable is an available means to enhance the mechanical characteristics of the alloy.

Heat treatment strengthening (solution treatment followed by rapid water quenching and subsequent artificial aging treatment) is a universal way to increase the strength of aluminum alloys. G.P. zones have a significant function in the heat treatment hardening mechanism. The first discovery of G.P. zones was made via X-ray diffraction of an Al-Cu alloy [2]. In Al-Mg alloys, the formation temperature for G.P. zones is about 0 °C. Therefore, for Al-Mg alloys, it is difficult to find G.P. zones during artificial aging. Sato et al. [3] found a modulated structure in an Al-10Mg alloy at the beginning of low-temperature aging, which grew into G.P. zones with $L1_2$ structures distributed periodically along the [100] direction. DSC analysis was employed to study the characteristics of these G.P. zones, and it was found that G.P. zones cannot immediately form after quenching. Long-term aging at room temperature led to the formation of a small quantity of G.P. zones [4]. When an alloy is heated at room temperature, aging behaviors can be mainly divided into two periods: G.P. zones and the β'' phase. The β'' phase has an $L1_2$ -type crystal lattice architecture and presents a completely coherent relationship with the Al-matrix [5]. It has a composition of Al_3Mg . The β'' phase is unstable in Al-Mg alloys and transforms into the β' phase at about 100 °C. It is generally accepted that the β' phase has a hexagonal lattice structure and is semi-coherent with the Al-matrix. The β' phase is reported in some research as the primary strengthening phase in Al-Mg alloys [6,7]. The equilibrium phase in Al-Mg alloys is the β phase (Al_3Mg_2), which has a face-centered cubic structure and is incoherent with the matrix. Based on wide research regarding the aging process in Al-Mg alloys, the precipitation sequence of the Al-Mg alloy has been summarized as follows [5,8–10]: Supersaturated solid solution (S.S.S.) \rightarrow G.P. zone \rightarrow β'' phase \rightarrow β' phase \rightarrow β phase. Due to the volatility of G.P. zones, coarse scaling, and sparsely distributed precipitate particles in Al-Mg alloys, the aging hardening response is limited for these alloys. Based on relevant research, 6061 aluminum alloy reached peak aging condition after aging at 200 °C for 200 min, and the presence of the β'' phase led to a significant increase in the yield strength of the alloy, greatly improving its mechanical properties [11].

According to reports, the addition of Ag can enhance the strength of Al-Cu-Mg alloys, resulting from the production of Mg-Ag clusters during the aging procedure [12]. Some scholars have also studied the influencing mechanism of Ag on the precipitation phase and precipitation sequence in Al-Mg alloys. It has been found that incorporating Ag in the Al-5Mg alloy can cause an obvious hardening [13]. The precipitation phase is known as the $T-Mg_{32}(Al, Ag)_{49}$ phase, as the lattice structure of this phase is very similar to that of the $Mg_{32}(Al, Zn)_{49}$ phase and Al_6CuMg_4 [14]. However, due to limitations in detection technology at the time, there was insufficient evidence to clearly demonstrate this.

In recent years, some researchers have studied the aging process in Al-Mg-Ag alloys and found that the addition of Ag has a marked impact on the precipitation particles. The hardness of the alloy was improved conspicuously using only small amounts of Ag [15,16]. However, these researchers mainly focused on 5xxx series aluminum alloys, which contained over 10 wt.% Mg. The effect of Ag on the microstructure of low magnesium content 5xxx series aluminum alloys has rarely been reported. If the aging temperature or the Mg content of the alloys is different, the precipitation order may slightly change [17]. Additionally, the effect of Ag on the microscopic structure and mechanical properties of Al-Mg alloys has also been rarely investigated.

In this study, to elucidate the framework of Ag in 5xxx aluminum alloys with low magnesium, the evolution of the microstructure of the as-cast, as-homogenized, as-rolled, as-quenched, and as-aged alloys is discussed in detail. The evolution of aging precipitates and the mechanistic effect of nano precipitates on the mechanical properties are illustrated in detail. Based on this study, a new method and foundation for exploiting new-type Al-Mg based alloys is provided. A novel method for developing high-strength aluminum alloys is also provided in this study.

2. Experimental

The investigated alloy, with the composition Al-4.5Mg-0.6Ag-0.7Mn-0.1Cr-0.1Zr (% by weight), was made via melting in an intermediate frequency furnace and casting into a copper mold. The raw materials for casting were commercial Al (99.7 wt.%), Mg (99.9 wt.%), Ag (99.9 wt.%), Al-10 wt.% Zr intermediate alloy, Cr agent, and Mn agent (75 wt.%). The as-cast ingot was homogenized at 500 °C for 24 h. Following this, hot rolling and cold rolling were employed to process the ingot into an alloy sheet with a thickness of 2 mm. The hot rolling temperature used was 450 °C, with a deformation factor of 70%. The deformation factor associated with cold rolling was 67%. The solid solution temperature of the alloy plate was 500 °C, and the insulation time was 2 h. Cooling was then performed using water (solution heat treatment). Artificial aging temperatures were 120 °C, 160 °C, 210 °C, and 270 °C, and the aging times were 0.5 h, 1 h, 2 h, 4 h, 8 h, 16 h, 24 h, and 32 h.

The microstructure of the alloy was characterized using optical microscopy (OM, Olympus, Japan), scanning electron microscopy (ultra-plus SSX-550 SEM, Kyoto, Japan) matching energy dispersive spectroscopy instruments (EDS, Oxford Instruments, Abingdon, UK), and transmission electron microscopy (TEM, JEM-ARM200F, Shimadzu Company, Kyoto, Japan).

The microstructure characterization was prepared by using a standard EDM cutting machine. The microstructural characterization specimens were rubbed with 240#, 1000#, and 3000# sandpaper, and then polished using silica polishing suspensions with particle sizes of 3 µm and 0.02 µm. To prepare the TEM samples, the alloy was first formulated into a circular plate with a diameter of 3 mm and a thickness of 80 µm, and then the circular plate was subjected to twin-jet electropolishing treatment. The electrolyte comprised a blended solution consisting of nitric acid and methanol in a 1:2 ratio. The voltage for electrolytic treatment was 15 V and the temperature was −25 °C.

For the preparation of polarized light images, samples were treated using an anode coating experiment. A regulated power supply with a voltage of 20 V was used to connect the cathode of the power supply to a lead block. The electrolyte solution was fluoroboric acid with a volume fraction of 1:16 in water. During anode coating, the sample was partially immersed in the electrolyte and controlled at a current density of 0.2 A for 60 s.

The measurement of the hardness of aged alloys was carried out using a Vickers hardness testing instrument (Qness, Q10A+, Golling, Austria). The hardness results reflected the average of 5–7 testing points under a load of 0.5 kg and a loading duration of 15 s. The mechanical properties of the investigated alloys were measured utilizing a universal testing machine of the CSS-44100 type (Changchun Testing Machine Factory, Changchun, China) following the GB/T16865-2013 standard condition of room temperature. The gage dimensions of tensile specimens were 50 mm × 12.5 mm, and the incipient strain rate of $6 \times 10^{-4} \text{ s}^{-1}$ was utilized. The sample dimensions for the tensile tests are shown in Figure 1. The traction measurements were performed three times to obtain their average value.

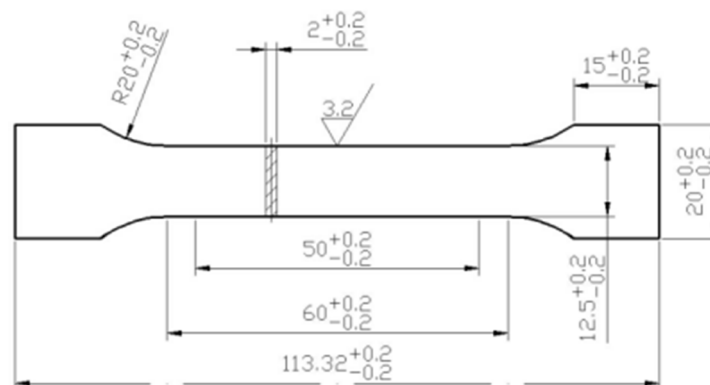


Figure 1. The size of tensile samples (mm).

3. Results

3.1. Microstructure

Figure 2 shows the microscopic structure of the as-cast Al-Mg-Mn-Ag-Cr-Zr alloy. As seen in the polarized light image in Figure 2a, the microstructure contains a large quantity of dendrites with significant diameter segregation. This is due to insufficient diffusion of elements during the solidification process. Figure 2b presents the OM image of the as-cast microstructure. The microstructure contains many second phases, which tend to connect along grain boundaries into a network. The corresponding SEM images are shown in Figure 2c,d. Two types of constituent phase were detected. One presented as bone-like with a coarse scale, and the other presented as bulk-like with a fine scale. The EDS results, which indicate the composition of the phases, are shown in Table 1. The bone-like phase contained mainly Mn and Fe elements and can be speculated to be the $Al_6(Mn, Fe)$ phase (red arrows). The bulk-like phase contained mainly Mg and Ag elements and can be considered the $T-Mg_{32}(Al, Ag)_{49}$ phase.

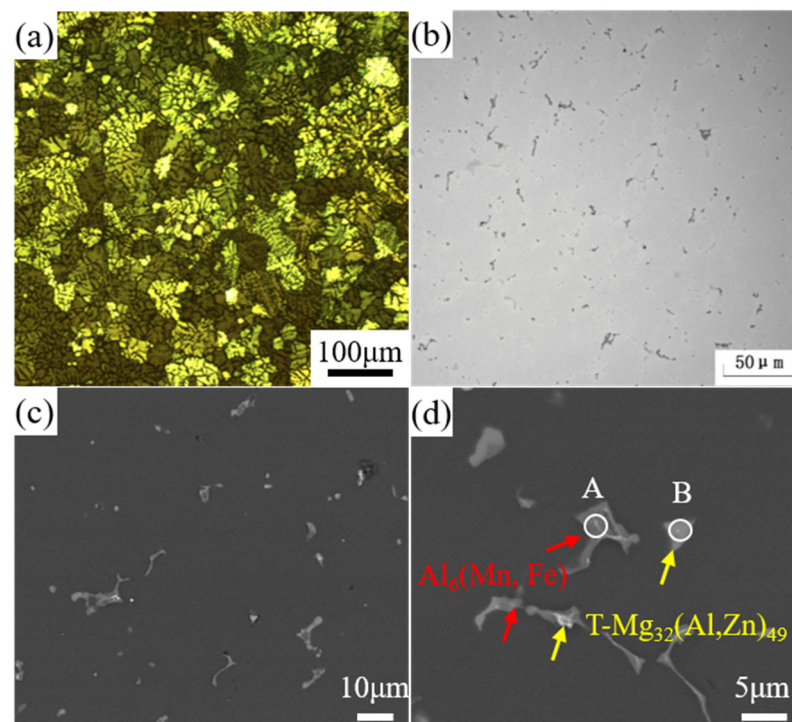


Figure 2. (a) Polarized light image (100 \times), (b) OM image (200 \times), and (c) SEM image of as-cast Al-Mg-Mn-Ag-Cr-Zr alloy (2000 \times); (d) enlarged SEM image (5000 \times) of (c).

Table 1. Composition of investigated phases in Figure 2 (wt.%).

Phase	Si	Mg	Mn	Cr	Fe	Ag	Al
A	0.9	2.3	15.4	0.9	10.6	1.2	Balance
B	2.1	24.3	-	-	-	21.2	Balance

To eliminate dendritic segregation of the as-cast microscopic structure, and improve the processing performance of the alloy, homogenization treatment was employed in this study. Figure 3 shows the micro-morphology of the as-homogenized Al-Mg-Mn-Ag-Cr-Zr alloy homogenized at 500 $^{\circ}C$ for 24 h. As shown in Figure 3a, the dendritic segregation was eliminated and numerous nanoscale particles precipitated from the matrix. Figure 3b,c present the SEM images of the distribution of the second phases. In contrast with the as-cast microstructure, the fraction of particles in the homogenized alloy decreased greatly. The coarse scale bone-like phases dissolved, transformed into small-sized phases, and

distributed along grain boundaries. To identify the composition of particles, the EDS mapping is shown in Figure 3d. From the images presented in Figure 3, results show that the coarse scale phases are the Mg_2Si phase (red arrows) and the $T-Mg_{32}(Al, Ag)_{49}$ phase (yellow arrows). The analysis of phase composition is also shown in Table 2. The $Al_6(Mn, Fe)$ phase and the fine-scale $T-Mg_{32}(Al, Ag)_{49}$ phase can also be detected in the as-homogenized microstructure.

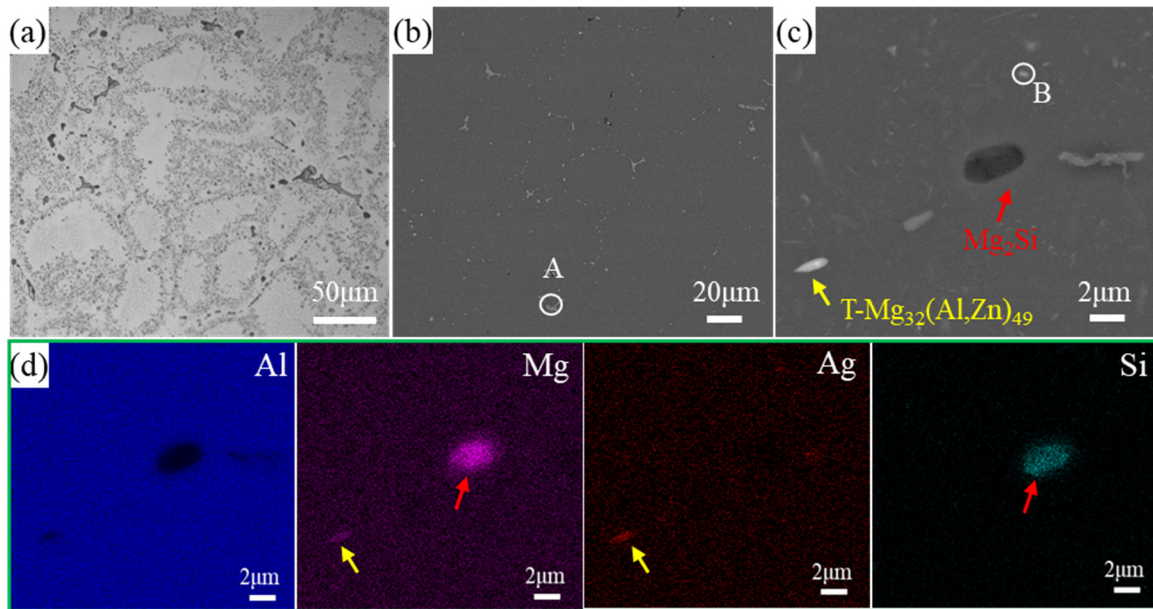


Figure 3. Microstructure of the alloy after homogenizing. (a) OM image (200×), (b) (1000×) and (c) (10,000×) SEM image; (d) EDS mapping results of (c). (The yellow arrows indicate the T phase while the red arrows represent the Mg_2Si phase.)

Table 2. Composition of investigated phases in Figure 3 (wt.%).

Phase	Mg	Mn	Fe	Ag	Al
A	0.6	9.9	13.3	0.6	Balance
B	8.1	-	-	12.9	Balance

Figure 4a,b represent the polarized light picture and the SEM picture of the alloy after cold rolling. As shown in Figure 4a, the microstructure contained typical fiber structures and deformation textures after cold rolling. Figure 4b shows that many coarse cracked gray intermetallic phases ($Al_6(Mn, Fe)$) and extremely fine dispersoids ($Mg_{32}(Al, Ag)_{49}$) distributed in alignment along the rolling direction. However, in Figure 4c, recrystallization has occurred, and the fiber structures have transformed to fine equiaxed grains after solute treatment at 500 °C for 2 h. The TEM image of the as-quenched alloy in Figure 4d shows that only the coarse scale $Al_6(Mn, Fe)$ phase distributed in the Al-matrix sparsely, while the fine scale dispersoids dissolved. The coarse scale particles are shown to have little effect on the aging strengthening process.

3.2. Precipitation Behavior of the Investigated Al-Mg-Mn-Ag-Cr-Zr Alloy

Figure 5 presents the evolution of the hardness of the Al-Mg-Mn-Ag-Cr-Zr alloy, which was aged at 120 °C, 160 °C, 210 °C, and 270 °C for 0–32 h. At the lower aging temperature of 120 °C, the hardness of the alloy increased gradually with the extension of aging time. As the aging temperature progressively rose, a discernible trend emerged in the hardness of the alloy, manifesting as an initial augmentation succeeded by a subsequent diminution as the aging duration extended. In addition, it is evident from Figure 5 that as the aging temperature increased, the rate of increase in alloy hardness also accelerated. The alloy

reached its maximum hardness when aged for 2 h, 4 h, 24 h, and 32 h, at 270 °C, 210 °C, 160 °C, and 120 °C, respectively. Through a comparative analysis of the maximum hardness values attained by the alloy at various aging temperatures, it becomes apparent that the alloy exhibited its most pronounced aging strengthening effect at 160 °C, reaching a peak hardness value of 117.3 HV. The increase in hardness during aging is related to the uniform precipitation of nanoscale particles. The hardness results indicate the appearance of nano phases in the microstructure during the aging process of the alloy, indicating that the alloy has a significant aging strengthening effect compared to traditional 5xxx series aluminum alloys. The specific precipitation microstructure will be introduced in the following results.

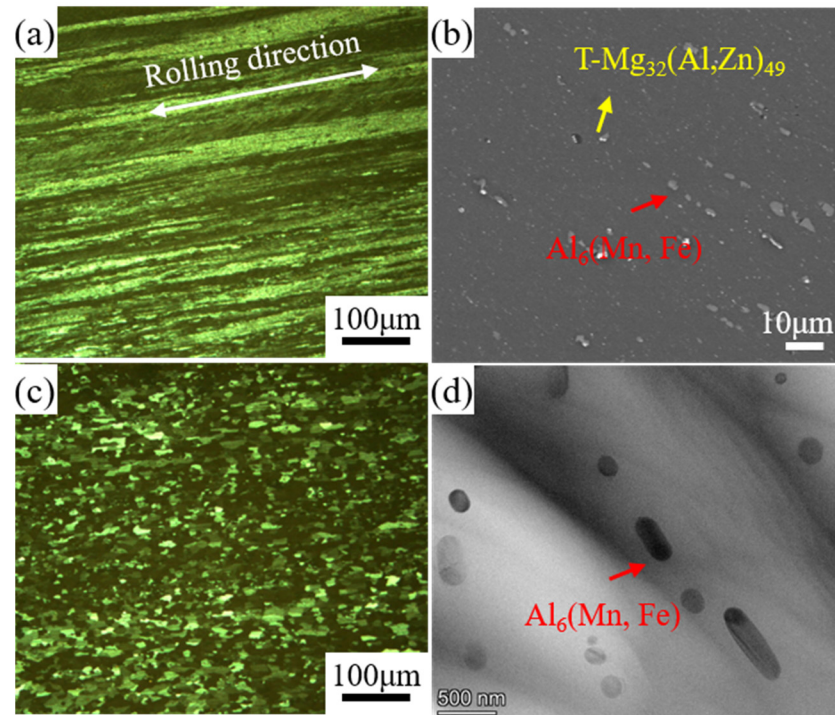


Figure 4. Microstructure of the alloy. (a) Polarized light picture of the alloy after cold rolling (100 \times), (b) SEM picture of the alloy after cold rolling (2000 \times), (c) polarized light picture of the as-quenched alloy (100 \times), (d) TEM image of as-quenched alloy.

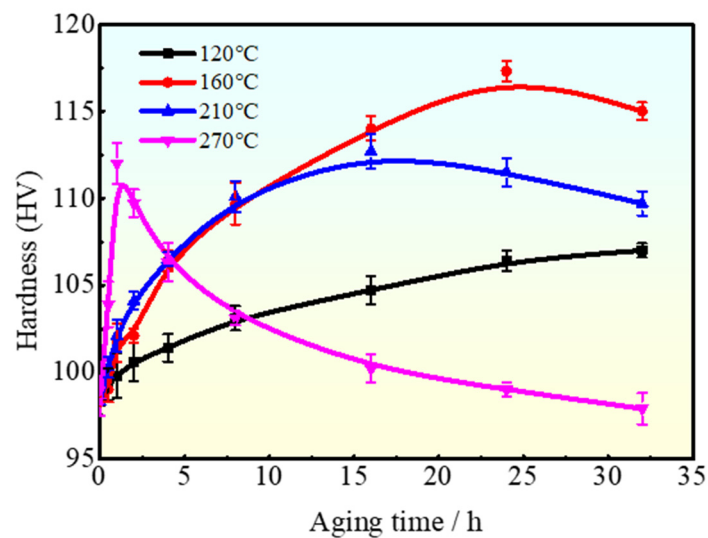


Figure 5. Hardness curves of Al-Mg-Mn-Ag-Cr-Zr alloy aged for 0–32 h at 120 °C, 160 °C, 210 °C, and 270 °C.

The evolution of aging precipitates plotted against aging temperature and time is shown in Figure 6. Figure 6a represents the TEM image of the Al-Mg-Mn-Ag-Cr-Zr alloy that was subjected to an aging heat treatment for 8 h at 160 °C. During the under-aged period, a large number of dot-like phases precipitated from the matrix and were dispersed within the grains homogeneously. The dimension of the precipitates was less than 2 nm, and these can be speculated to have been G.P. zones at this stage. These G.P. zones had no independent lattice structure and were completely coherent with the matrix. The strengthening effect of the G.P. zones was mainly caused by lattice distortion energy between solute atoms and matrix atoms.

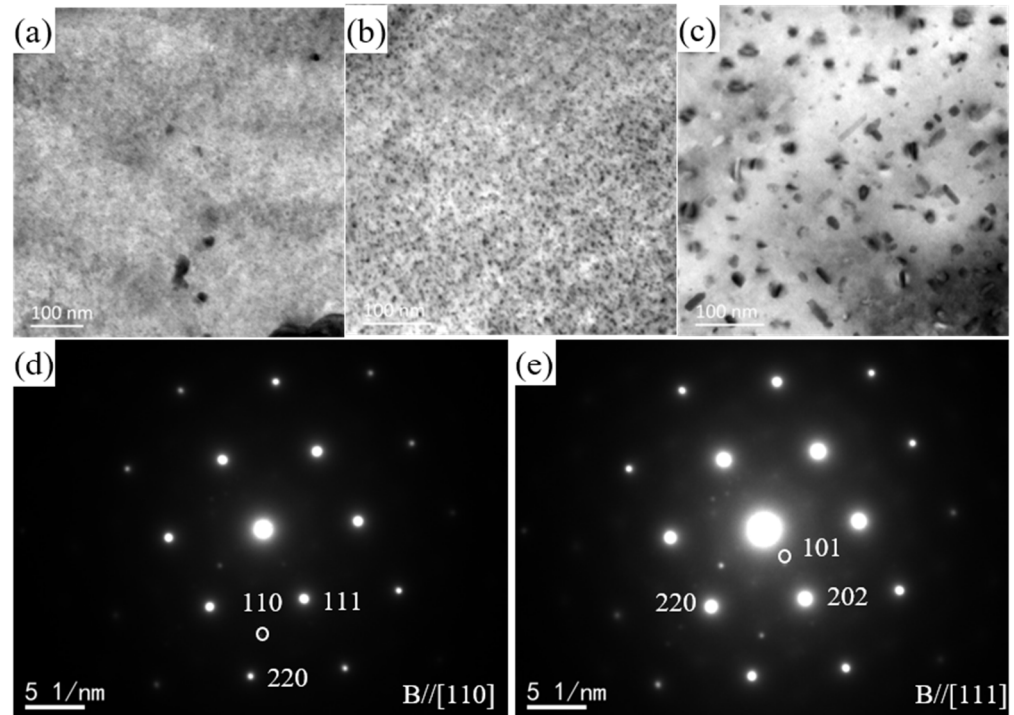


Figure 6. TEM images of the Al-Mg-Mn-Ag-Cr-Zr alloy (a) aged for 8 h at 160 °C, (b) aged for 24 h at 160 °C, and (c) aged for 16 h at 270 °C. (d,e) show the SAED patterns along the $[110]_{\alpha}$ and (c) $[111]_{\alpha}$ zone axis.

Figure 6b presents the TEM image taken at the peak-aged period of the investigated alloy, aged at 160 °C for 24 h. The microstructure continued to comprise numerous finely dispersed, circular precipitate particles uniformly distributed within the matrix. In comparison to the under-aged stage, the precipitates at the peak-aged stage exhibited increased coarseness, accompanied by a substantially higher volume fraction. The rise in volume fraction of precipitates had an improved effect on hindering dislocation movements and thus improved the strength of the alloy. Corresponding selected area electron diffraction (SAED) images of the precipitates are shown in Figure 6d,e. Based on the calibration results of the diffraction patterns, the precipitates had a $L1_2$ -type lattice structure. The lattice parameter, a , of the precipitates was 0.408 nm. These results are in accordance with the lattice parameter of the β'' phase (Al_3Mg) [10]. In addition, as Ag is the main element promoting the precipitation of nano phases, the precipitates definitively contained a proportion of elemental Ag. Therefore, the composition of this precipitate can be inferred as $Al_3(Mg, Ag)$.

The HRTEM images in Figure 7 show the interface between the matrix and the β'' particles. The precipitations are coherent with the matrix. However, there is obvious lattice distortion and an elastic strain zone within the particles. The HAADF-STEM image in Figure 7b shows the atomic arrangement of the aging precipitates. Since the brightness of an atomic column is directly proportional to the square of the atomic number (Z^2), Ag atom columns (which are brighter owing to Ag's higher atomic number) are distributed

around the edge of the precipitate phase, while Mg atoms are concentrated in the center of the precipitate phase, forming a “core-shell” structure. With a further elongation of aging time, when the alloy aged for 32 h at 160 °C, as shown in Figure 5, the hardness of the alloy exhibited minimal variation when compared to the peak-hardness stage. This reflects that the precipitate particles were thermally stable at 160 °C, and the alloy did not reach the over-aged period owing to the limited aging treatment time.

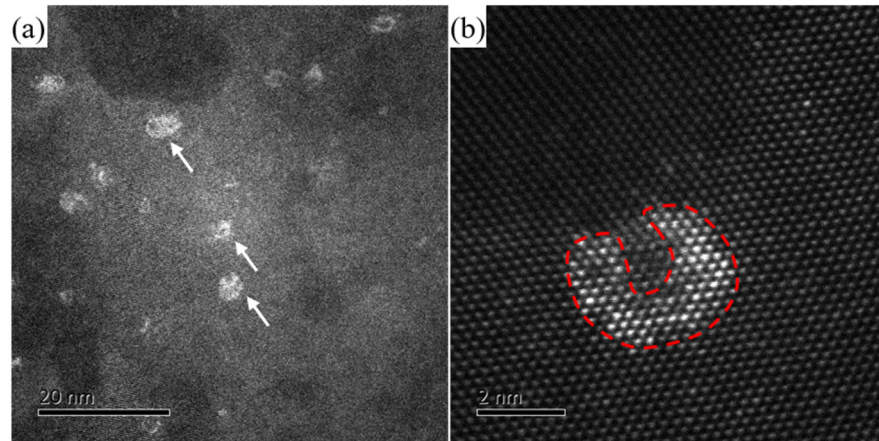


Figure 7. (a) HRTEM image and (b) atomic-scale HAADF-STEM image of aging precipitates. (The white arrows refer to the nanoscale precipitates. The red dashed lines show the structure of the precipitates).

The alloy reached the over-aged stage after being subjected to aging for 16 h at a temperature of 270 °C. The morphology of the precipitates at this stage is shown in Figure 6c. The precipitates underwent a transformation into rod-shaped particles, distributing themselves evenly within the matrix, and exhibiting dimensions ranging from 20 to 50 nanometers. As a result, it can be assumed that the precipitated rod-shaped phases are of the T phase, with their primary composition being $Mg_{32}(Ag, Al)_{49}$ [18].

The mechanical properties of the investigated alloys are presented in Figure 8. The as-quenched alloy demonstrated a yield strength (YS) of 273 MPa and an ultimate tensile strength (UTS) of 410 MPa, accompanied by an elongation rate of 26%. For the peak-aged alloy (aged at 160 °C for 24 h), strength is significantly improved. The yield strength (YS) measured at 273 MPa, marking a 47.5% increase compared to the YS of the as-quenched alloy. Similarly, the ultimate tensile strength (UTS) stood at 449 MPa, reflecting a 9.5% enhancement over the UTS of the as-quenched alloy. The alloy additionally maintained good ductility, with an elongation rate of 22%. The measured improvements in alloy strength occurred mainly due to the strong pinning effect of the relative dislocations of the nano β'' phase in the alloy and the plastic deformation process, which substantially improved the strength characteristics of the alloy. During the aging treatment process, the number and density of precipitated phases gradually increased, pinning dislocations and grain boundaries, hindering dislocation movement, and thus improving mechanical strength. Therefore, the change in the number of precipitates at the grain boundaries of the microstructure is also an important factor in the mechanical properties of the alloy [19].

For the as-aged alloys, the increase in strength of increment precipitates can be reflected by using the Orowan hardening model following the formula [20]:

$$\Delta\sigma_{pre} = 0.84M \frac{Gb}{\lambda_d} \quad (1)$$

where $M = 3.06$ is the Taylor factor, $G = 27$ GPa is the shear modulus, $b = 0.286$ nm is the magnitude of the Burgers vector, and λ_d is the mean distance between precipitates. λ_d is calculated by the following formula [21]:

$$\lambda_d = 6d_p \sqrt{\frac{2\pi}{v_p}} \quad (2)$$

where d_p is the average diameter of the precipitates, and v_p is counted as the area fraction. Owing to the higher v_p and lower d_p of precipitates in the peak-aged alloy than that of the as-quenched alloy, the mechanical characteristics of the peak-aged alloy are significantly greater than that of the as-quenched alloy (UTS increases by 9.5%, YS increases by 47.5%).

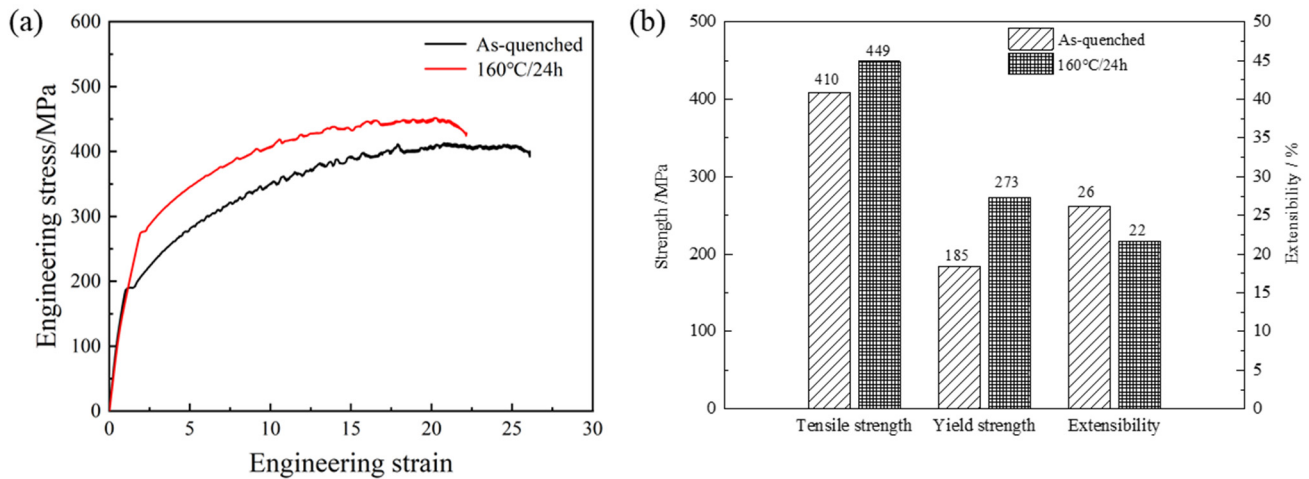


Figure 8. Engineering stress-strain curves (a) of the as-quenched and peak-aged alloys and corresponding UTS, YS, and (b) elongation.

4. Discussion

In addressing the challenge of insufficient hardening during heat treatment of 5xxx aluminum alloys and trying to improve the mechanical characteristics of these alloys, a new Al-Mg-Mn-Ag-Cr-Zr alloy was developed. The addition of Ag influenced microstructural evolution, and the alloy performance is dictated by the characteristics of microstructure. Through adjusting the aging heat treatment procedure parameters, the alloy demonstrated an apparent aging-strengthening function.

As shown in Figure 5, the hardness of the novel Al-Mg-Mn-Ag-Cr-Zr alloy increases significantly during the aging heat treatment procedure. The hardness of the alloy at its peak-aged state surpasses that of the as-quenched alloy by an increment of 19 HV. This hardening response can be attributed to the precipitation of numerous nanoscale particles during artificial aging. As is well known, Al-Mg based alloys have little aging hardening response owing to the absence of stable G.P. zones. As the nearest atomic spacing difference between Al (2.862 Å) and Mg (3.196 Å) is significant, the solid solution of Mg atoms in the aluminum matrix produce significant lattice distortion, which can lead to the unstable aggregation of Mg atoms. The lack of G.P. zones thus results in insufficient nucleating positions for the nano phases, making it difficult for the precipitated phase to nucleate. The Al-Mg based alloy therefore does not present an obvious aging strengthening response.

Comparatively speaking, as represented in Figures 6 and 7, the microstructure of the novel Al-Mg-Mn-Ag-Cr-Zr alloy consists of a lot of nanoscale precipitates, which distributed in the grains homogeneously. The addition of Ag can facilitate precipitation. During the solid solution treatment process, Ag increased the concentration of quenched vacancies in the investigated alloy, thereby ameliorating the aging precipitation kinetics of the alloy. In addition, as Mg and Ag atoms have strong binding energy, in the initial period of aging, Mg and Ag atoms gradually aggregate to form Ag-Mg clusters [22,23]. The Ag-Mg clusters can function as nucleation sites, thereby facilitating the nucleation and subsequent precipitation of nanoscale strengthening phases. Additionally, because the atomic radii of the Ag atom and Al atom differ by only 0.5%, the lattice distortion energy between atomic clusters and the matrix is relatively small. The Ag-Mg clusters can

thus maintain a stable state in aluminum matrix at the initial aged period. This also leads to a higher number of clusters and G.P. zones in the novel Al-Mg-Mn-Ag-Cr-Zr alloy as compared to the traditional Al-Mg based alloy.

When the Al-Mg-Mn-Ag-Cr-Zr alloy reaches the peak-aged stage, as shown in Figure 6b, the dimensions and volume fraction of these precipitates both increase, and at this point, the precipitates transform from the Mg-Ag G.P. zones to the β'' phase that is coherent with the matrix. Meanwhile, so as to diminish the distortion energy between the coherent β'' phase and the matrix, Ag atoms diffuse towards the edges of the precipitates, while Mg atoms are distributed in the center of the precipitates. As a result, the precipitates present a “core-shell” structure, as shown in Figure 7b. The stable β'' phase with fine scale and large density has a great pinning effect and is able to hinder the movement of dislocations, which enhances the mechanical characteristics of the alloy in the ductility deformation procedure. The incorporation of Mn, Cr, and Zr elements in the investigated alloy can serve as ternary additions. During the heat treatment procedure, randomly distributed dispersed phases can precipitate, pin grain boundaries and inhibit grain growth, improve grain stability, and thus enhance alloy plasticity [24]. Ternary addition of elements has a synergistic strengthening effect in the β'' phase, ensuring acceptable plasticity of the alloy while assuring high mechanical strength.

Compared with the as-quenched alloy, the YS of the investigated alloy at the peak-aged period increased by 47.5%. This reflects the great strengthening effect of the β'' phase. Due to the significant discrepancy in atomic extent between Mg atoms and Al/Ag atoms in the center of the precipitates, the precipitates also exhibited significant distortion energy with the matrix. This also promoted an increase in strength. However, as shown in Figure 8, this increase in strength did not result in a significant decrease in ductility of the alloy. This is attributed to the refined grain size observed in the alloy following the solution treatment, as depicted in Figure 4c. When the aging time of the alloy is extended to 32 h, there is no obvious decrease in hardness. This is because the interface energy between the β'' phase and the matrix is relatively small, which keeps the precipitates stable and less prone to coarsening. Therefore, the precipitates still have a good effect on pinning dislocations, and the alloy maintains a high hardness.

In order to demonstrate the microstructural characteristics during the over-aged period, the alloy underwent an aging procedure at 270 °C for a duration of 16 h. At this stage, the dimensions of the precipitates underwent significant coarsening, and the number of precipitates declined significantly, as presented in Figure 6c. The coarsening process of precipitates acts to reduce the interfacial energy between precipitates and the matrix, and to transform the transition phase into a stable phase [25]. As a result, the coherent β'' phase transforms to the T phase at the over-aged stage [26,27].

5. Conclusions

In this study, to improve the age-hardening response of Al-Mg-based alloys, an investigation into the microstructural evolution and mechanical properties of a new Al-Mg-Mn-Ag-Cr-Zr alloy was carried out. From the results of the investigations carried out in this study, the following conclusions can be drawn:

- (1) In regard to the as-cast alloy, the microstructure contained a large number of dendrites with significant diameter segregation. The second phase consisted of the T-Mg₃₂(Al, Ag)₄₉ phase and the Al₆(Mn, Fe) phase.
- (2) After homogenization, the dendritic segregation was eliminated and numerous nanoscale phases formed in the Al-matrix. The microstructure contained typical fiber structures and deformation textures after cold rolling. The fiber structures transformed into fine equiaxed grains after solute treatment.
- (3) During the aging procedure, the addition of Ag assisted the precipitation of the β'' phase, which nucleated on the Mg-Ag clusters. The β'' phase had a L1₂-type lattice structure and presented a completely coherent relevance with the Al-matrix. The lattice parameter, *a*, of the β'' phase was 0.408 nm. The β'' phase presented a “core-

shell" structure as Ag atoms diffused towards the edges of the precipitates, while Mg atoms were distributed in the center of the precipitates.

- (4) The mechanical properties of the alloy in the peak-aged period improved greatly as compared to that of the as-quenched alloy. The tensile strength grew from 410 MPa to 449 MPa while the yield strength increased from 185 MPa to 273 MPa, an increase of 9.5% and 47.5%, respectively.

Author Contributions: Conceptualization, C.G.; Methodology, H.W. and T.L.; Investigation, T.L. and Y.W.; Writing—original draft, H.W.; Writing—review and editing, C.G. All authors have read and agreed to the published version of the manuscript.

Funding: This research received no external funding.

Institutional Review Board Statement: Not applicable.

Informed Consent Statement: Not applicable.

Data Availability Statement: Data are contained within the article.

Conflicts of Interest: Author Tao Liu and Yanli Wu were employed by the MCC Heavy Industry (Tangshan) Co., Ltd. The remaining authors declare that the research was conducted in the absence of any commercial or financial relationships that could be construed as a potential conflict of interest.

References

1. He, L.Z.; Li, X.H.; Liu, X.T.; Wang, X.J.; Zhang, H.T.; Cui, J.Z. Effects of homogenization on microstructures and properties of a new type Al-Mg-Mn-Zr-Ti-Er alloy. *Mater. Sci. Eng. A* **2010**, *527*, 7510–7518. [\[CrossRef\]](#)
2. Preston, G.D. The Diffraction of X-rays by age-hardening aluminum copper alloys. *Proc. R. Soc. A* **1938**, *167*, 526–538.
3. Sato, T.; Kojima, Y.; Takahashi, T. Modulated structures and G.P. zones in Al-Mg alloys. *Metall. Trans. A* **1982**, *13*, 1373–1378. [\[CrossRef\]](#)
4. Boucheur, M.; Hamana, D.; Laoui, T. GP zones and precipitate morphology in aged Al-Mg alloys. *Philos. Mag. A* **1996**, *73*, 1733–1740. [\[CrossRef\]](#)
5. Yang, W.C.; Wang, M.P.; Jia, Y.L.; Zhang, R.R. Studies of orientations of β'' precipitates in Al-Mg-Si-(Cu) alloys by electron diffraction and transition matrix analysis. *Metall. Mater. Trans. A* **2011**, *42*, 2917–2929. [\[CrossRef\]](#)
6. Jeong, H.T.; Kim, W.J. Strain hardening behavior and strengthening mechanism in Mg-rich Al-Mg binary alloys subjected to aging treatment. *Mater. Sci. Eng. A* **2020**, *794*, 139862. [\[CrossRef\]](#)
7. Fukui, K.; Watanabe, R.; Takeda, M. Morphology and thermal stability of metastable precipitates formed in an Al-Mg alloy aged at 373K and 473K. *Appl. Mech. Mater.* **2015**, *799*, 212–216. [\[CrossRef\]](#)
8. Yang, M.J.; Chen, H.N.; Orekhov, A.; Lu, Q.; Lan, X.Y.; Li, K.; Zhang, S.Y.; Song, M.; Kong, Y.; Schryvers, D.; et al. Quantified contribution of β'' and β' precipitates to the strengthening of an aged Al-Mg-Si alloy. *Mater. Sci. Eng. A* **2020**, *774*, 138776. [\[CrossRef\]](#)
9. Ninive, P.H.; Strandlie, A.; Gulbrandsen-Dahl, S.; Lefebvre, W.; Marioara, C.D.; Andersen, S.J.; Friis, J.; Holmestad, R.; Løvvik, O.M. Detailed atomistic insight into the β'' phase in Al-Mg-Si alloys. *Acta Mater.* **2014**, *69*, 126–134. [\[CrossRef\]](#)
10. Wei, Z.J.; Jiang, W.; Zou, C.M.; Wang, H.W.; Zhao, W.Q. Microstructural evolution and mechanical strengthening mechanism of the high pressure heat treatment (HPHT) on Al-Mg alloy. *J. Alloys Compd.* **2017**, *692*, 629–633. [\[CrossRef\]](#)
11. Ozturk, F.; Sisman, A.; Toros, S.; Kilic, S.; Picu, R.C. Influence of aging treatment on mechanical properties of 6061 aluminum alloy. *Mater. Des.* **2010**, *31*, 972–975. [\[CrossRef\]](#)
12. Chen, M.C.; Chung, T.F.; Tai, C.L.; Chen, Y.H.; Yang, J.R.; Lee, S.L.; Hsiao, C.N.; Tsao, C.S.; Chou, C.M. Quantitative evaluation of the effect of Ag-addition on the concurrently-existing precipitation kinetics in the aged Al-Cu-Mg (-Ag) alloys. *Mater. Des.* **2023**, *227*, 111766. [\[CrossRef\]](#)
13. Mihara, M.; Marioara, C.D.; Andersen, S.J.; Holmestad, R.; Kobayashi, E.; Sato, T. Precipitation in an Al-Mg-Cu alloy and the effect of a low amount of Ag. *Mater. Sci. Eng. A* **2016**, *658*, 91–98. [\[CrossRef\]](#)
14. Guo, C.; Zhang, H.T.; Wu, Z.B.; Wang, D.T.; Li, B.M.; Cui, J.D. Effects of Ag on the age hardening response and intergranular corrosion resistance of Al-Mg alloys. *Mater. Charact.* **2019**, *147*, 84–92. [\[CrossRef\]](#)
15. Kubota, M.; Muddle, B.C. Effect of trace additions of Ag on precipitation in Al-Mg alloys. *Mater. Trans.* **2005**, *46*, 2968–2974. [\[CrossRef\]](#)
16. Kubota, M.; Feng, N.J.; Chales, M.B. Characterisation of precipitation hardening response and as-quenched microstructure in Al-Mg(-Ag) Alloys. *Mater. Trans.* **2004**, *45*, 3256–3263. [\[CrossRef\]](#)
17. Yi, G.; Littrell, K.C.; Poplawsky, J.D.; Cullen, D.A.; Sundberg, E.; Freea, M.L. Characterization of the effects of different tempers and aging temperatures on the precipitation behavior of Al-Mg (5.25 at.%) -Mn alloys. *Mater. Des.* **2017**, *118*, 22–35. [\[CrossRef\]](#)
18. Guo, C.; Zhang, H.T.; Wu, Z.B.; Shen, X.D.; Wang, P.; Li, B.M.; Cui, J.Z.; Nagaumi, H. An atomic-resolution investigation of precipitation evolution in Al-Mg-Ag alloys. *Mater. Lett.* **2019**, *248*, 231–235. [\[CrossRef\]](#)

19. Ercetin, A. Application of the hot press method to produce new Mg alloys: Characterization, mechanical properties, and effect of Al addition. *J. Mater. Eng. Perform.* **2021**, *30*, 4254–4262. [[CrossRef](#)]
20. Wen, H.; Topping, T.; Isheim, D.; Seidman, D.; Lavernia, E. Strengthening mechanisms in a high-strength bulk nanostructured Cu-Zn-Al alloy processed via cryomilling and spark plasma sintering. *Acta Mater.* **2013**, *61*, 2769–2782. [[CrossRef](#)]
21. Sahoo, B.; Das, D.; Chaubey, A. Strengthening mechanisms and modelling of mechanical properties of submicron-TiB₂ particulate reinforced Al 7075 metal matrix composites. *Mater. Sci. Eng. A* **2021**, *825*, 141873. [[CrossRef](#)]
22. Sato, T. Nanocluster Control for Achieving High Strength Aluminum Alloys. *Mater. Trans.* **2018**, *59*, 861–869. [[CrossRef](#)]
23. Wang, Y.C.; Wu, X.D.; Cao, L.F.; Tong, X.; Zou, Y.; Zhu, Q.Q.; Tang, S.B.; Song, H.; Guo, M.X. Effect of Ag on aging precipitation behavior and mechanical properties of aluminum alloy 7075. *Mater. Sci. Eng. A* **2021**, *804*, 140515. [[CrossRef](#)]
24. Maeng, D.Y.; Lee, J.H.; Hong, S.I. The effect of transition elements on the superplastic behavior of Al-Mg alloys. *Mater. Sci. Eng. A* **2003**, *357*, 188–195. [[CrossRef](#)]
25. Wang, J.; Shin, S.; Nobakht, A.; Shyam, A. Structural deformation and transformation of θ' -Al₂Cu precipitate in Al matrix via interfacial diffusion. *Comput. Mater. Sci.* **2019**, *156*, 111–120. [[CrossRef](#)]
26. Senapati, S. Evolution of Lamellar Structures in Al-Ag Alloys. Master's Thesis, University of Central Florida, Orlando, FL, USA, 2005.
27. Kubota, M.; Nie, J.F.; Muddle, B.C. Identification of metastable rod-like particles in an isothermally aged Al-10Mg-0.5Ag (mass%) alloy. *Mater. Trans.* **2005**, *46*, 1288–1294. [[CrossRef](#)]

Disclaimer/Publisher's Note: The statements, opinions and data contained in all publications are solely those of the individual author(s) and contributor(s) and not of MDPI and/or the editor(s). MDPI and/or the editor(s) disclaim responsibility for any injury to people or property resulting from any ideas, methods, instructions or products referred to in the content.